

Comparative analysis for detecting areas with building damage from several destructive earthquakes using satellite synthetic aperture radar images

Masashi Matsuoka^a and Fumio Yamazaki^b

^aNational Institute of Advanced Industrial Science and Technology, Site 2, 1-1-1 Umezono, Tsukuba, Ibaraki 305-8568, Japan

m.matsuoka@aist.go.jp

^bChiba University, 1-33 Yayoi-cho, Inage-ku, Chiba, Chiba 263-8522, Japan

fumio.yamazaki@faculty.chiba-u.jp

Abstract. Earthquakes that have caused large-scale damage in developed areas, such as the 1994 Northridge and 1995 Kobe events, remind us of the importance of making quick damage assessments in order to facilitate the resumption of normal activities and restoration planning. Synthetic aperture radar (SAR) can be used to record physical aspects of the Earth's surface under any weather conditions, making it a powerful tool in the development of an applicable method for assessing damage following natural disasters. Detailed building damage data recorded on the ground following the 1995 Kobe earthquake may provide an invaluable opportunity to investigate the relationship between the backscattering properties and the degree of damage. This paper aims to investigate the differences between the backscattering coefficients and the correlations derived from pre- and post-earthquake SAR intensity images to smoothly detect areas with building damage. This method was then applied to SAR images recorded over the areas affected by the 1999 Kocaeli earthquake in Turkey, the 2001 Gujarat earthquake in India, and the 2003 Boumerdes earthquake in Algeria. The accuracy of the proposed method was examined and confirmed by comparing the results of the SAR analyses with the field survey data.

Keywords: earthquake, building damage, SAR, backscattering coefficient, ERS, Radarsat.

1 INTRODUCTION

Obtaining an accurate overview of large-scale natural disasters in metropolitan areas of developing countries can be difficult. Although quick damage estimation systems, such as strong ground motion monitoring and/or flow monitoring by utilities, may be available, a time lag between the initial damage estimation and the actual damage assessment is unavoidable. Furthermore, we expect damage assessment to take longer as the extent of damage increases. In order to properly respond to a disaster, it is essential to make decisions even as damage assessment information continues to be accumulated, striking a balance between timeliness and accuracy. Observations of damaged areas by helicopter, airplane, and satellite provide information to fill in initial quick damage estimates with actual damage assessments that are timely, cover a large area, and have high accuracy, respectively. In particular, remote sensing by satellites can provide observations of a wide area with a single image, and it may be possible to use this technology to improve the accuracy of large-scale damage estimates [1,2].

To apply remote sensing technology to quantify damage in the aftermath of a natural disaster, it is preferable to use simple and universally applicable methods that have a minimal processing time, without the need to rely on actual ground survey data. Synthetic aperture radar (SAR), a type of radar used for remote sensing, is an active system that measures the backscattering intensity and phase information of microwaves reflected from the Earth's surface [3]. High-resolution remote sensing using SAR is one of the most promising

technologies for monitoring damaged areas [4–8]. Unlike passive optical sensors, SAR enables observation of surface conditions day or night, and through clouds. More importantly, intensity information obtained from SAR yields a physical value, the backscattering coefficient, which is strongly dependent on the roughness of the ground surface and the dielectric constant. This means that changes on the Earth’s surface can be measured not in relative but in absolute terms. The variance of the backscattering coefficient can be calculated as a representation of the level of building damage on the target ground surface. In addition, it may be possible to apply this method to a wide range of areas with different observation environments.

Based on these ideas, we developed a method to map areas with building damage by clarifying the relationship between changes in the backscattering coefficient in pre- and post-earthquake satellite SAR data and the building damage assessment based on detailed field investigations following the 1995 Kobe earthquake [9]. In order to confirm the applicability of the rapid damage detection at a practical level where no field survey data are available, it is necessary to test this method by applying it to other destructive earthquakes. Accordingly, we have applied the method to earthquakes in Kocaeli, Turkey (1999), Gujarat, India (2001), and Boumerdes, Algeria (2003) without using calibration samples.

2 BUILDING DAMAGE DETECTION METHOD USING SAR DATA

SAR directs microwave radiation at the surface of the Earth at a downward slanting angle sideways to the azimuth direction of a platform, such as an airplane or a satellite. Then, the backscattering intensity and phase of the microwaves reflected from the surface are collected. Therefore, SAR can be used to obtain images that are completely different from those of optical sensor satellite images, which are produced by observing the reflection and radiation characteristics of visible and infrared electromagnetic waves from objects on the Earth.

The magnitude of the backscattering intensity is affected by the wavelength and incident angle of the microwaves and the roughness and dielectric characteristics of the ground surface. When the focus is placed only on the roughness, microwave data may be employed for urbanized areas which have larger backscattering intensities due to multiple reflections, a phenomenon called the "cardinal effect between structures and the ground." On the other hand, microwaves aimed at areas with collapsed buildings or open space produce less backscattering because the scattering of the microwaves is then more multi-directional. Based on these characteristics, we have developed a method for detecting areas with severely damaged buildings using time-series SAR datasets for the Kobe earthquake [9].

The dataset obtained following the 1995 Kobe earthquake demonstrated that the damage to an area could be expressed as the difference between pre- and post-earthquake backscattering coefficients and their correlation coefficient. The basic principle of this detection method is that the level of building damage is related to the backscattering coefficient. To examine the damaged area, the following steps are performed. First, two multi-look intensity images are prepared: one taken before the earthquake and the second taken after. The interval between acquisition dates should be as short as possible and the observation conditions should be similar. However, the damage assessment images of the Kobe earthquake that were used as the image pair were taken from very different satellite observation orbits. After co-registering the pre- and post-earthquake images, each image is filtered using a Lee filter [10] with a 21×21 pixel window. The difference in the backscattering coefficient d in Eq. (1) and the correlation coefficient r in Eq. (2) is derived from the two filtered images, and the discriminant score z in Eq. (3) is obtained by linear regression analysis using calibration samples of field survey data from the Kobe earthquake [9],

$$d = 10 \cdot \log_{10} \bar{I}a_i - 10 \cdot \log_{10} \bar{I}b_i , \quad (1)$$

$$r = \frac{N \sum_{i=1}^N I_{a_i} I_{b_i} - \sum_{i=1}^N I_{a_i} \sum_{i=1}^N I_{b_i}}{\sqrt{\left(N \sum_{i=1}^N I_{a_i}^2 - \left(\sum_{i=1}^N I_{a_i} \right)^2 \right) \cdot \left(N \sum_{i=1}^N I_{b_i}^2 - \left(\sum_{i=1}^N I_{b_i} \right)^2 \right)}}, \quad (2)$$

$$z = -2.140 d - 12.465 r + 4.183, \quad (3)$$

where i is the sample number, and I_{a_i} and I_{b_i} are the digital numbers of the pre- and post-earthquake images, respectively. \bar{I}_{a_i} and \bar{I}_{b_i} are the corresponding numbers of pixels surrounding pixel i within a 13×13 pixel window; the total number of pixels N within this window is 169, which is used to compute the two indices. A pixel with a high z value is interpreted as showing a severely damaged area. Focusing on detection of building damage within urbanized areas, pixels with backscattering coefficients smaller than an assigned threshold value of approximately -5 to -6 dB are masked in the z value distribution.

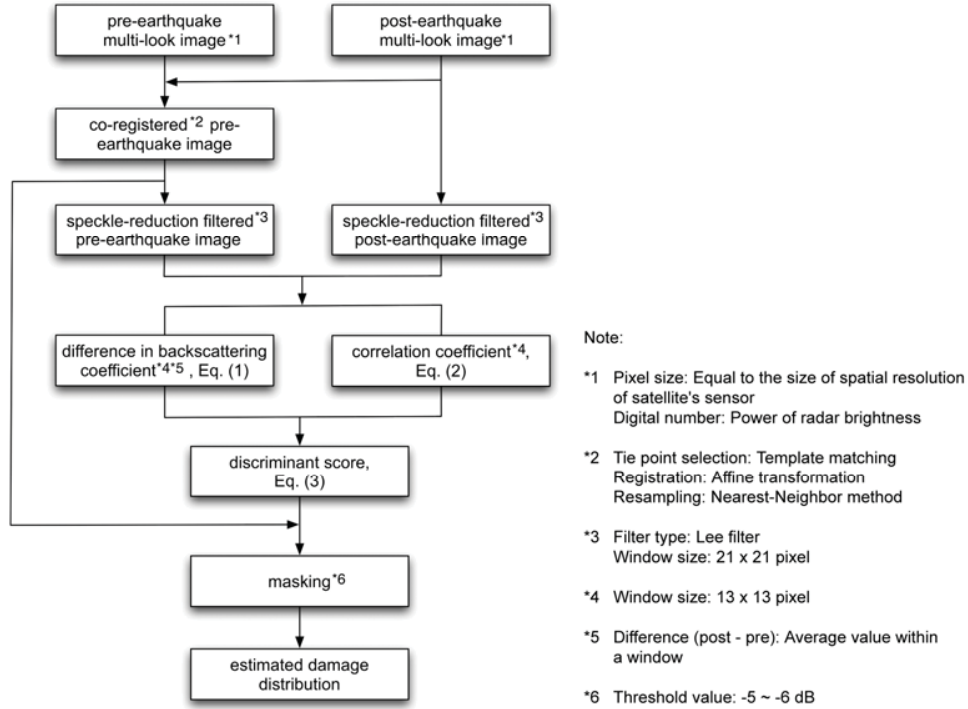


Fig. 1. Flowchart and notes for image processing to detect areas with building damage.

The filter and window sizes used are empirically determined to reduce speckle noise and increase the accuracy of damage interpretation based on comparisons between ERS-1 (Earth Resources Satellite-1) images of pixel size 30 m and building damage survey data [11], sorted by city blocks following the Kobe earthquake. These optimal values may be dependent on the condition of the urban area and the spatial resolution of the corresponding satellite image. We use the optimized values from the Kobe earthquake data in this study to investigate whether the proposed method is applicable to damaged areas, even in the absence of specific information pertaining to those areas. A flow chart outlining the method is shown in Fig. 1.

3 EARTHQUAKES AND SAR DATA

Satellite SAR images of several areas recently stricken by destructive earthquakes are available. We applied the described method to the 1999 Kocaeli, Turkey, the 2001 Gujarat, India, and the 2003 Boumerdes, Algeria earthquakes and compared the results with field investigation reports and detailed building damage assessment data.

On August 17, 1999, a moment magnitude (M_w) 7.4 earthquake shook the northwestern Kocaeli region of Turkey, causing severe damage over a wide area around Izmit. Deaths totaled 17,000 and more than 77,000 houses were completely destroyed [12]. A series of ERS-1 and ERS-2 radar observations conducted over the affected area before (August 13) and after (September 17, 1999) the event were used as pre- and post-earthquake images. The image area used in the analysis is shown in Fig. 2. Because the perpendicular separation of the two satellites, called the baseline length B_p , was approximately 30 m, this pair is also perfectly suitable for an interferometric study and for coherence analysis of damage interpretation [13,14].

One-and-a-half years later, the Gujarat earthquake (M_w 7.5) devastated the western part of India on January 26, 2001. An extremely wide area from Bhuj, near the seismic source, to Ahmadabad, located 300 km away, was affected. According to the Indian Government, 20,000 people died and 720,000 houses were completely destroyed. A Canadian satellite, Radarsat-1, which has a fine-beam mode with ground (pixel) resolution of approximately 8 m and an incident angle of 46° , recorded an image during a flight path over Bhuj city on February 11, 2001 (Fig. 3). We used an image taken on December 31, 1999, as the pre-earthquake image. This pair of images were separated by a time interval of more than 400 days and the B_p of the two acquisitions was more than 6 km, making this image pair a poor prospect for being able to detect damage using the coherence of phase information.

An M_w 6.8 earthquake shook the Mediterranean coast of Algeria on May 21, 2003. The epicenter was located offshore of the province of Boumerdes. The cities of Boumerdes and Zemmouri, which are located approximately 50 to 60 km east of the capital city of Algiers, were most extensively damaged. Approximately 7,400 buildings collapsed and an additional 7,000 were heavily damaged. ERS-2 observed the hardest-hit areas of Boumerdes and Zemmouri on June 7, 2003. An image acquired on July 27, 2002 was used for the pre-earthquake image. The image area used in analysis is shown in Fig. 4. The baseline length B_p between the two satellite positions was more than 1 km.

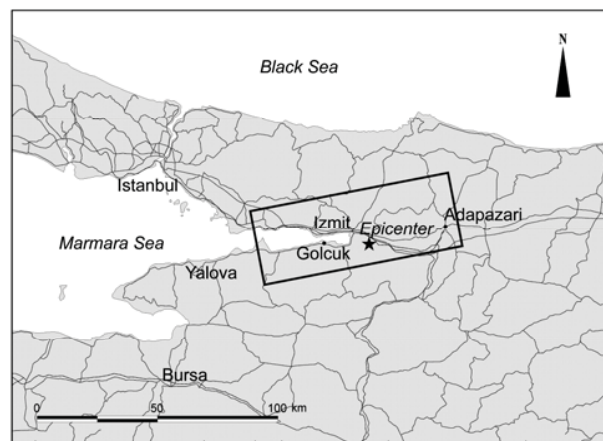


Fig. 2. Area analyzed for the 1999 Kocaeli, Turkey earthquake. The area inside the rectangle indicates the region of interest in the ERS image.



Fig. 3. Area analyzed for the 2001 Gujarat, India earthquake. The area inside the rectangle indicates the region of interest in the Radarsat/Fine image.

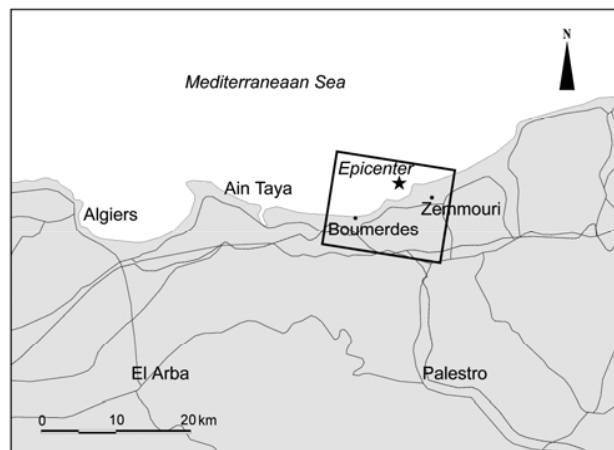


Fig. 4. Area analyzed for the 2003 Boumerdes, Algeria earthquake. The area inside the rectangle indicates the region of interest in the ERS image.

4 DAMAGE DETECTION AND COMPARISON WITH ACTUAL DAMAGE

4.1 1999 Kocaeli, Turkey earthquake

The result of overlaying the distribution of discriminant score z on the pre-earthquake image is shown in Fig. 5. To limit the area of study to urbanized areas, the threshold value was set at -6 dB. Damaged areas, shown in red, are widely detected in Golcuk and Adapazari, but not in other cities around Izmit Bay. This distribution is in good agreement with the damage statistics obtained by a survey made one week after the earthquake [15]. However, the unit of aggregation in this survey was not systematic and varies by neighborhood, block, and city. Therefore, we cannot say that these data accurately indicate damage levels, but they do serve as a good overview of the damage.

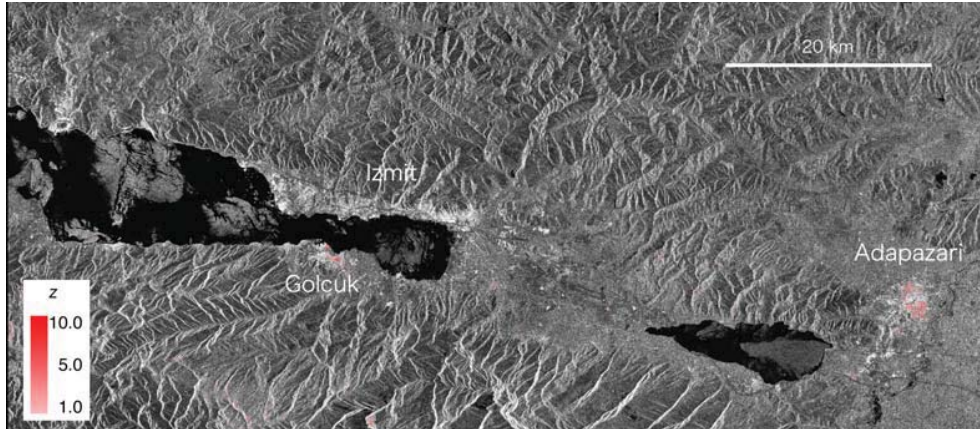


Fig. 5. Distribution of z values calculated from a pair of ERS images taken on 1999/8/13 and 1999/9/17 of the area affected by the 1999 Kocaeli, Turkey earthquake.

In Golcuk, a Japanese survey team conducted a detailed, systematic field survey of building damage [12]. The building collapse rate, which is the ratio of buildings suffering Grade 5 damage on the European Macroseismic Scale (EMS) [16] in Golcuk, was classified into areas with 0–6.25, 6.25–12.5, 12.5–25, 25–50, and 50–100% damage on the scale of the city block [17]. These data are overlaid on the damage map derived using SAR (Fig. 6). Sunken areas along the coast are excluded from the analysis in the masking process; therefore, no damage pixels (shown in black) are detected there. In other highly damaged areas, many damage pixels can be observed.

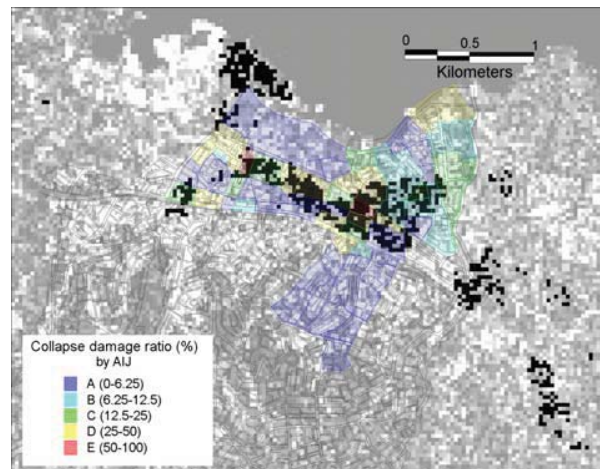


Fig. 6. Building damage areas derived from SAR images (discriminant scores z larger than 1 are in black) and field survey data [17] in Golcuk, Turkey.

The mean and standard deviation of the discriminant score z by damage level, including that for the Kobe earthquake [9], are shown in Table 1. After the Kobe earthquake, collapsed buildings were not surveyed precisely, and the approximate rate of "severely damaged" buildings is given in Table 1. "Severe damage" corresponds to a range that includes Grade 5, Grade 4 and a portion of Grade 3 damage in the EMS system [18]. Though the standard deviations vary widely, the tendency for the mean of z to be larger as the damage level increases is common to both earthquakes. The mean of z is slightly greater for Golcuk than

for Kobe. Judging from the differences in the backscattering coefficient and the correlation coefficient shown in Table 1, the small correlation coefficient in Golcuk influences the value of z . As explained above, the criteria for building damage differs in the two cases, and collapsed buildings generate greater surface changes than do severely damaged buildings. There is a 0.1 difference in the correlation coefficient in areas where the damage level is 0–6.25%. The fact that the structures in the two areas were not equivalent and that most of the Kobe metropolitan area was paved whereas there were more unpaved areas in Golcuk makes the observed surface change in Golcuk appear larger.

Damage statistics for Adapazari were reported by the Turkish government. The distribution of damage rates calculated from the data [19] is overlaid on the damage map extracted from SAR images (Fig. 7). Here, the damage rate represents the ratio of damaged buildings and corresponds to EMS ranks Grade 5 through Grade 3. We cannot compare the damage rate and extracted pixels directly because there are areas with extremely small numbers of buildings [19]. We can, however, observe that the areas with high damage rates correspond to dense distributions of pixels that represent damage. As shown in Table 1, the greater the damage rate, the larger the z value. On October 2, following the earthquake, we visually surveyed damaged areas in Adapazari from a vehicle [20]. Table 1 shows the z value of the survey results for damage classified into three categories (no damage to slight damage, moderate to heavy damage, and catastrophic damage). A similar correspondence between the damage level and z value can be seen.

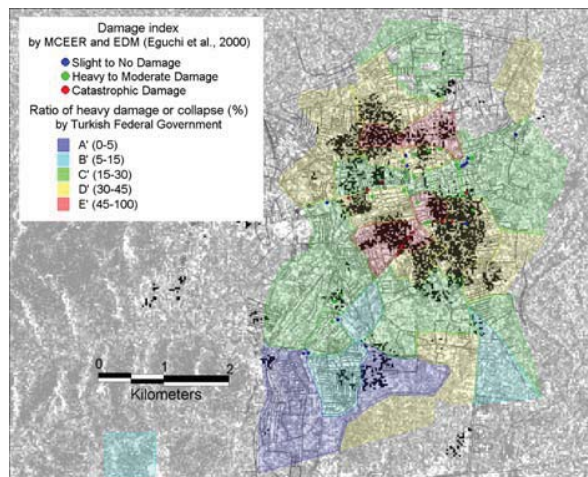


Fig. 7. Building damage areas derived from SAR images (discriminant score z larger than 1 is in black) and field survey data [19,20] from Adapazari, Turkey.

4.2 2001 Gujarat, India earthquake

The application of our damage detection method to the Radarsat-1/Fine images is shown in Fig. 8. In urban areas, the extraction threshold value is -6 dB. The analysis identifies local areas of damage in Bhuj, Anjar and in some villages between the two cities. Even with the long baseline length B_p , these results correspond well to damage assessments made from aerial photographs [21] and from Landsat images [22]. A high-resolution satellite, IKONOS, which has a swath width of 11 km and a ground resolution of 1 m, made observations of the surroundings of Bhuj two days after the earthquake. The relationship between the estimated damage areas from the post-earthquake IKONOS images [23] and calculated z values is shown in Table 1.

Table 1. Mean and standard deviation of differences in backscattering coefficient, correlation, and discriminant scores by damage level.

Earthquakes and analyzed areas	No. of pixels	Mean and standard deviation		
		d [dB]	r	z
1995 Kobe, Japan				
Hanshin area				
(severe damage ratio) [11]				
0–6.25%	2000	-0.29 (0.35)	0.54 (0.14)	-1.96 (2.02)
6.25–12.5%	2000	-0.37 (0.43)	0.50 (0.15)	-1.24 (2.30)
12.5–25%	2000	-0.54 (0.47)	0.48 (0.16)	-0.60 (2.44)
25–50%	2000	-0.71 (0.60)	0.43 (0.17)	0.32 (2.85)
50–100%	2000	-0.95 (0.79)	0.36 (0.18)	1.70 (3.41)
1999 Kocaeli, Turkey				
Golcuk				
(collapse damage ratio) [17]				
0–6.25%	363	-0.36 (0.30)	0.44 (0.14)	-0.55 (1.74)
6.25–12.5%	117	-0.13 (0.30)	0.40 (0.21)	-0.54 (2.66)
12.5–25%	140	-0.49 (0.47)	0.41 (0.16)	0.13 (2.21)
25–50%	218	-0.69 (0.27)	0.36 (0.15)	1.21 (1.85)
50–100%	24	-1.01 (0.07)	0.33 (0.13)	2.18 (1.61)
Adapazari				
(heavy damage or building collapse rate) [19]				
0–5%	666	0.07 (0.29)	0.46 (0.21)	-1.65 (2.38)
5–15%	589	-0.01 (0.19)	0.46 (0.14)	-1.49 (1.81)
15–30%	2967	-0.04 (0.27)	0.43 (0.14)	-1.07 (1.77)
30–45%	2799	-0.30 (0.29)	0.33 (0.13)	0.74 (1.68)
45–100%	1102	-0.40 (0.28)	0.32 (0.10)	1.07 (1.30)
Adapazari				
(damage level) [20]				
No damage to slight damage	13	-0.10 (0.20)	0.46 (0.12)	-1.30 (1.63)
Moderate to heavy damage	25	-0.16 (0.36)	0.40 (0.10)	-0.43 (1.64)
Catastrophic damage	10	-0.53 (0.20)	0.28 (0.06)	1.81 (1.01)
2001 Gujarat, India				
Bhuj (building damage level) [23]				
Areas without extensive or complete damage	6743	-0.17 (0.91)	0.32 (0.14)	0.58 (2.52)
Extensive damage	1011	-0.80 (0.91)	0.30 (0.11)	2.13 (2.69)
Complete damage	738	-0.92 (0.78)	0.28 (0.11)	2.66 (2.43)
Bhuj (severe damage ratio) [2]				
0–25%	1283	-0.09 (0.82)	0.33 (0.13)	0.29 (2.65)
25–50%	856	-0.68 (0.58)	0.39 (0.14)	0.69 (2.52)
50–75%	1591	-0.99 (0.90)	0.32 (0.13)	2.25 (2.92)
75–100%	2440	-0.78 (0.81)	0.30 (0.11)	2.10 (2.36)
2003 Boumerdes, Algeria				
Zemmouri (collapse damage ratio) [24]				
0–6.25%	27	-0.04 (0.15)	0.61 (0.04)	-3.38 (0.70)
6.25–12.5%	6	-0.34 (0.07)	0.51 (0.03)	-1.45 (0.54)
12.5–25%	18	-0.51 (0.23)	0.37 (0.10)	0.71 (1.77)
25–50%	16	-0.80 (0.05)	0.33 (0.05)	1.79 (0.74)
50–100%	0	–	–	–

In Bhuj, a damage survey was carried out by Environmental Planning Collaborative (EPC), a nonprofit organization, and a $100\text{ m} \times 100\text{ m}$ grid square resampled damage map was examined [2]. Overlaying it on the results of the estimate obtained using SAR images, we calculated the z value of each damage level, which is also listed in Table 1. The z value demonstrates the degree of building damage and is relatively close to the results determined in the analysis of Golcuk. Indeed, the urban district structure and damage pattern of the buildings in India are similar to those in Turkey.

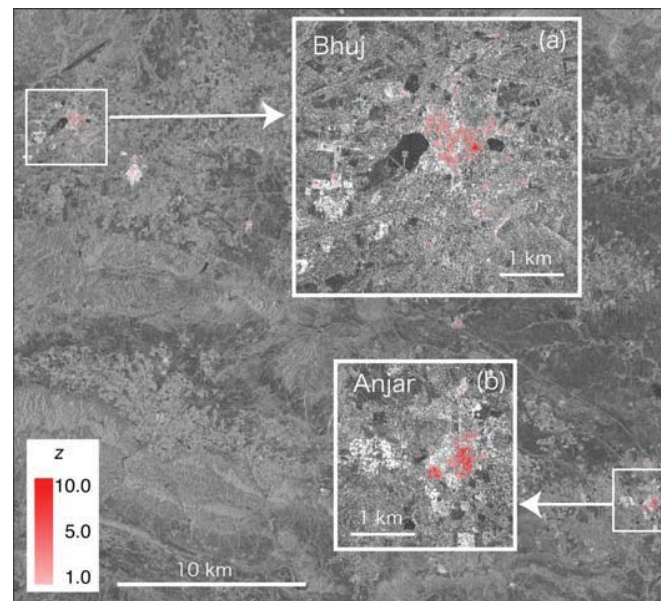


Fig. 8. Distribution of z values calculated from a pair of Radarsat/Fine images taken on 1999/12/31 and 2001/2/11 of the area affected by the 2001 Gujarat, India, earthquake.

4.3 2003 Boumerdes, Algeria earthquake

The distribution of the discriminant score z are calculated for the earthquake using our damage detection method and ERS-2 images. The threshold value of the backscattering coefficient for selected built-up areas is -6 dB . The distribution of z values is shown in Fig. 9. Our examinations of the 1995 Kobe, 1999 Turkey, and 2003 India earthquakes empirically suggest that areas where the building collapse rate is greater than approximately 25% can be detected for a range of z values set to be greater than one.

We were not able to extract a wide distribution of building damage in Boumerdes. Visual inspection of building damage there was conducted based on EMS classifications using pre- and post-earthquake images obtained by the QuickBird satellite [24]. In that study, the ratio of damaged Grade 5 buildings in each city block was calculated and the maximum value of the damage ratio was not very high, about 14%. Therefore, this result for Boumerdes agrees well with the application of our method to other earthquakes.

Damaged areas in the city of Zemmouri are shown in red on the map in Fig. 9. In Zemmouri, building damage ratios were calculated by five interpreters, who are researchers and graduate students in the fields of structural engineering, using QuickBird images [24]. The distribution of d , r , and z values is overlaid on the pre-earthquake SAR intensity image, georectified and compared with GIS-based visual inspection data. Mean values and standard deviations of d and r for different damage levels based on the ratio of buildings with Grade 5

damage in Zemmouri are also shown in Table 1. We found that in heavily damaged areas, the difference in the backscattering coefficient, d , is high and negative, and the correlation coefficient, r , is low. As observed in the Kobe, Turkey, and India cases, the z value in the Algeria case also increases as the damage level increases.

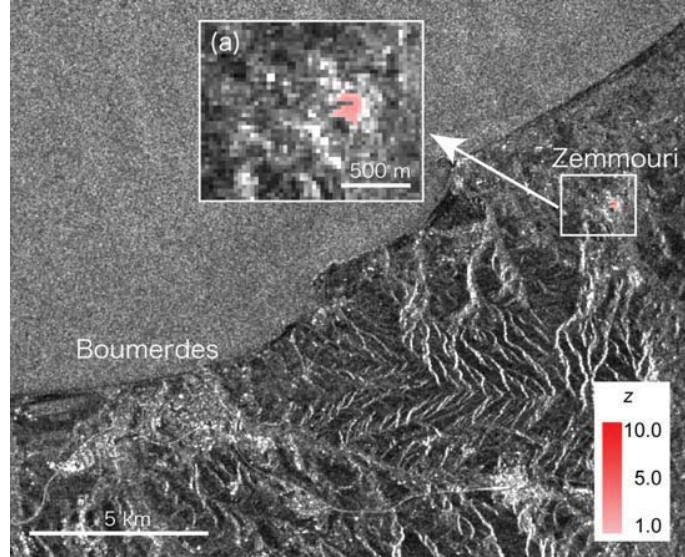


Fig. 9. Distribution of z values calculated from a pair of ERS images taken on 2002/7/27 and 2003/6/7 of the area affected by the 2003 Boumerdes, Algeria, earthquake.

5 OBSERVATIONS

In the above discussions, we confirmed that, for destructive earthquakes, building damage produces a reduced backscattering coefficient on SAR images. The correlation coefficient between the pre- and post-earthquake images also decreases. Therefore, the average z value derived from the backscattering coefficient differences and the correlation coefficients increases as the damage rank increases, though the standard deviations are too wide to predict the rank of damage that individual buildings may have suffered (Fig. 10). However, in the case of the 2003 Bam, Iran earthquake, analysis of pre- and post-earthquake SAR images produced results that were the reverse of this relationship in some severely damaged areas in the southeastern part of the city. The backscattered echoes from severely damaged areas in which there had been densely packed but orderly houses with flat roofs increased in the image taken after the earthquake [25]. The particular conditions created from this special environment did not exist elsewhere in our preliminary analysis [26]; therefore, we only consider cases in which the backscattering coefficient decreases in the post-earthquake images for the damage detection process we describe here.

For comparison purposes, we used calibration samples from field survey data [12] to conduct supervised classification using linear regression discriminant analysis and to calculate optimal discriminant scores, z_{Turkey} , for Golcuk, Turkey, as shown in Eq. (4).

$$z_{\text{Turkey}} = -5.660 d - 6.583 r , \quad (4)$$

The relationship between the damage rank and z_{Turkey} is shown in Fig. 11. Although this simulation also shows large standard deviations, the ability to identify damage rank is better than in the case shown in Fig. 10. In particular, lower damage ranks (A and B) can be

separated from the more severe damage rank E. Supervised damage detection shows good results even in the case of linear analysis if we have field survey data. Non-linear classification algorithms such as neural networks will be able to produce better results. Further studies using comparative approaches to select suitable damage detection schemes from among image classification methods are needed.

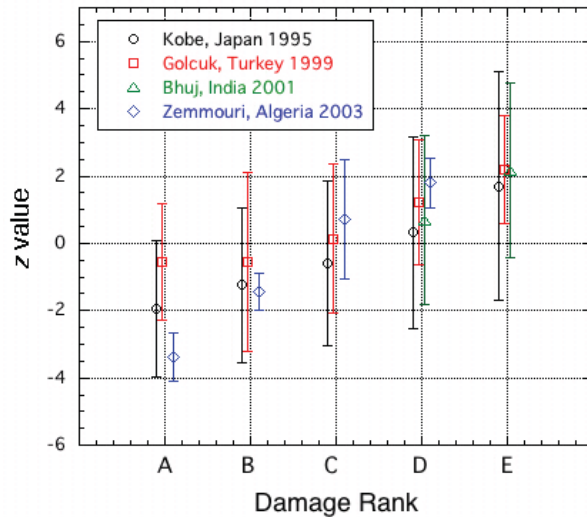


Fig. 10. Relationship between damage rank and discriminant score z . Damage ranks A to E are classified as areas in which, respectively, 0–6.25, 6.25–12.5, 12.5–25, 25–50, and 50–100% of buildings have suffered severe damage.

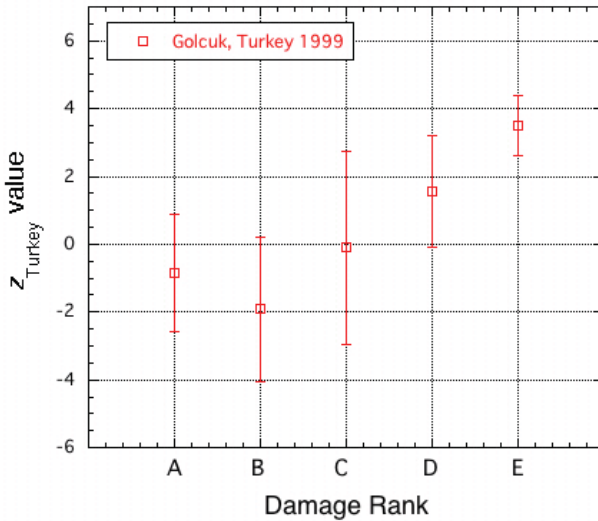


Fig. 11. Relationship between damage rank and optimal discriminant score z for the Turkey earthquake calculated from calibration samples. Damage ranks A to E are classified as areas in which, respectively, 0–6.25, 6.25–12.5, 12.5–25, 25–50, and 50–100% of buildings have suffered severe damage.

As shown in Fig. 5 for the Turkey earthquake, our method produces some pixels indicating damaged areas around mountain ridges. These misinterpretations extend wider as

we reduce the threshold value to less than -6 dB to mask areas without buildings. These pixels are a result of the "foreshortening effect", which is due to the relationship between the slope of the ground and the incident angle of the microwaves. In such areas, the backscattering intensity is similar to that observed in urbanized areas, and the masking process is ineffective. Here, we simply selected the area subject to analysis by a masking process based on the backscattering coefficient. When an urban area can be specified beforehand by interpretation of optical sensor images or existing GIS data, this type of error can be avoided. In urban areas where errors are more pronounced, it is thought that changes in ground surface roughness due to factors other than earthquake damage are picked up. Differences in pre- and post-earthquake observation conditions may also affect the results of our method.

In order to develop a more accurate damage detection method, it is necessary to compare detailed data on differences in satellite orbits as well as atmospheric and surface moisture and local site conditions. We plan to clarify the accuracy and limitations of our method through theoretical observations [27] using backscattering characteristic simulations that take into account the cardinal effect between structures and bare ground surfaces.

6 CONCLUSION

In this paper, we introduced a building damage mapping method based on comparisons of field survey data and satellite SAR intensity images obtained before and after the 1995 Kobe earthquake. We applied the method to other destructive earthquakes, including the 1999 Kocaeli, Turkey, the 2001 Gujarat, India, and the 2003 Boumerdes, Algeria earthquakes, in order to validate the appropriateness of the method. In these earthquakes, damaged areas were detected based on a compound variable that uses differences and correlations of the backscattering coefficient as explanatory variables that roughly correspond to the distribution of severely damaged buildings as obtained by field investigations and/or interpretation of high resolution satellite images. We also confirmed that this technique is not highly dependent on the type of built-up environment or the baseline length between the pre- and post-earthquake satellite images.

In the future, we will investigate the feasibility of damage detection under different observation conditions (microwave frequency, incident angle, and ground resolution) before and after an earthquake, and for using multiple SAR satellites to increase the observation frequency.

Acknowledgments

Discussions with Mr. R. Eguchi, Mr. C. Huyck, and Dr. B. Mansouri of ImageCat, Inc. were helpful to this study. We would also like to express our gratitude to the European Space Agency (ESA) for ERS and the Canadian Space Agency (CSA) for Radarsat-1 images.

References

- [1] P. Gamba, A. Marazzi, and E. Costamagna, "Satellite data analysis for earthquake damage assessment," *Proc. SPIE* **3222**, 340–350 (1997) [doi:10.1117/12.298164].
- [2] K. Saito, R. J. S. Spence, C. Going, and M. Markus, "Using high-resolution satellite images for post-earthquake building damage assessment: A study following the 26 January 2001 Gujarat Earthquake," *Earthquake Spectra* **20**, 145–169 (2004) [doi:10.1193/1.1650865].
- [3] F. M. Henderson, and A. J. Lewis, *Principles and Applications of Imaging Radar, Manual of Remote Sensing*, **2**, Wiley, New York (1998).

- [4] C. Yonezawa and S. Takeuchi, "Decorrelation of SAR data by urban damages caused by the 1995 Hyogoken-nanbu earthquake," *Int. J. Remote Sens.* **22**, 1585–1600 (2001) [doi:10.1080/01431160118187].
- [5] G. A. Arciniegas, W. Bijker, N. Kerle, and V. A. Tolpekin, "Coherence- and amplitude-based analysis of seismogenic damage in Bam, Iran, using Envisat ASAR data," *IEEE Trans. Geosci. Remote Sens.* **45**, 1571–1581 (2007) [doi:10.1109/TGRS.2006.883149].
- [6] P. Gamba, F. Dell'Acqua, and G. Trianni, "Rapid damage detection in the Bam area using multitemporal SAR and exploiting ancillary data," *IEEE Trans. Geosci. Remote Sens.* **45**, 1582–1589 (2007) [doi:10.1109/TGRS.2006.885392].
- [7] L. Zhen, C. Quan, Z. Jianmin, and T. Bangsen, "Analysis of synthetic aperture radar image characteristics for seismic disasters in the Wenchuan earthquake," *J. Appl. Remote Sens.* **3**, 031685 (2009) [doi:10.1117/1.3153906].
- [8] G. Huadong, L. Xinwu, and Z. Lu, "Study of detecting method with advanced airborne and spaceborne synthetic aperture radar data for collapsed urban buildings from the Wenchuan earthquake," *J. Appl. Remote Sens.* **3**, 031695 (2009) [doi:10.1117/1.3153902].
- [9] M. Matsuoka, and F. Yamazaki, "Use of satellite SAR intensity imagery for detecting building areas damaged due to earthquakes," *Earthquake Spectra* **20**, 975–994 (2004) [doi:10.1193/1.1774182].
- [10] J. S. Lee, "Digital image enhancement and noise filtering by use of local statistics," *IEEE Trans. Pattern Analy. Machine Intell.* **2**, 165–168 (1980) [doi:10.1109/TPAMI.1980.4766994].
- [11] Building Research Institute (BRI), *Final Report of Damage Survey of the 1995 Hyogoken-Nanbu Earthquake*, Building Research Institute (1996) (in Japanese).
- [12] Architectural Institute of Japan (AIJ), Japan Society of Civil Engineers (JSCE), and The Japanese Geotechnical Society (JGS), *Report on the Damage Investigation of the 1999 Kocaeli Earthquake in Turkey*, Architectural Institute of Japan (1999).
- [13] M. Matsuoka and F. Yamazaki, "Use of interferometric satellite SAR for earthquake damage detection," *Proc. 6th International Conference on Seismic Zonation, Earthquake Engineering Research Institute*, pp.103–108 (2000).
- [14] B. Mansouri, B. Houshmand, and M. Shinozuka, "Building change/damage detection in Seymen, Turkey, using ERS SAR data," *Proc. SPIE* **4330**, 18–26 (2001) [doi:10.1117/12.434125].
- [15] L. A. Johnson, A. Coburn, and M. Rahnema, "Damage survey approach to estimating insurance losses," *Earthquake Spectra* **16**, 281–293 (2000) [doi:10.1193/1.1586156].
- [16] European Seismological Commission, *European Macroseismic Scale 1998 (EMS-98)*, GeoForschungsZentrum Potsdam, Germany. (1998).
- [17] Architectural Institute of Japan (AIJ) reconnaissance team (T. Kabeyasawa, et al.), "Progress report on damage investigation after Kocaeli earthquake by Architectural Institute of Japan," *Proc. ITU-IAHS International Conference on the Kocaeli Earthquake 17 August 1999*, Istanbul Technical University, pp.300–305 (1999).
- [18] N. Maki, K. Horie, H. Hayashi, and S. Tanaka, "Physical damage level comparison of the damage assessments results in the Hanshin-Awaji Earthquake Disaster," *J. Social Safety Sci.* **3**, 117–122 (2001) (in Japanese with English abstract).
- [19] J. D. Bray and J. P. Stewart, "Damage pattern and foundation performance in Adapazari," *Earthquake Spectra*, **16**, 163–189 (2000) [doi:10.1193/1.1586152].
- [20] R. T. Eguchi, C. K. Huyck, B. Houshmand, B. Mansouri, M. Shinozuka, F. Yamazaki, M. Matsuoka, and S. Ulgen, "The Marmara earthquake: A view from space, the Marmara Turkey earthquake of August 17, 1999," *Reconnaissance*

- Report, Technical Report MCEER-00-0001*, Multidisciplinary Center for Earthquake Engineering Research, pp.151–169 (2000).
- [21] R. Sinha, A. Goyal, M. Choudhury, K. Jaiswal, A. S. Arya, R. Shaw, J. Saita, H. Arai, and K. Pribadi, *The Bhuj earthquake of January 26, 2001, Consequences and Future Challenges*, Indian Institute of Technology Bombay and Earthquake Disaster Mitigation Research Center, NIED (2001).
- [22] Y. Yusuf, M. Matsuoka, and F. Yamazaki, "Damage detection after 2001 Gujarat earthquake using Landsat-7 satellite images," *J. Indian Soc. Remote Sens.* **29**, 17–22 (2001) [doi:10.1007/BF02989909].
- [23] L. Chiroiu and G. Andre, "Damage assessment using high resolution satellite imagery: Application to 2001 Bhuj, India, earthquake," *Proc. 7th National US Conference on Earthquake Engineering*, Earthquake Engineering Research Institute, 13p. CD-ROM (2002).
- [24] F. Yamazaki, K. Kouchi, M. Matsuoka, M. Kohiyama, and N. Muraoka, "Damage detection from high-resolution satellite images for the 2003 Boumerdes, Algeria earthquake," *Proc. 13th World Conference on Earthquake Engineering*, Earthquake Engineering Research Institute, No.2595, 13p. CD-ROM (2004).
- [25] M. Matsuoka and F. Yamazaki, "Building damage mapping of Iran earthquake using Envisat/ASAR intensity imagery," *Earthquake Spectra* **21**, S285–S294 (2005) [doi:10.1193/1.2101027].
- [26] M. Matsuoka, and F. Yamazaki, "Building damage detection using SAR intensity images for recent earthquakes," *Proc. 2004 Envisat & ERS Symposium, ESA SP-572*, European Space Agency, 6p. CD-ROM. (2004).
- [27] M. Shinozuka, R. Ghanem, B. Houshmand, and B. Mansouri, "Damage detection in urban areas by SAR imagery," *J. Eng. Mechan.* **126**, 769–777 (2000) [doi:10.1061/(ASCE)0733-9399(2000)126:7(769)].

Masashi Matsuoka is a senior research scientist at the National Institute of Advanced Industrial Science and Technology (AIST), Tsukuba, Japan. He received his BS degree in architectural engineering from Muroran Institute of Technology in 1990. In 1992 and 1996, respectively, he received his MS and PhD degrees in the engineering of the built environment, both from the Tokyo Institute of Technology. He was with the Remote Sensing Technology Center at the Tokyo Institute of Technology and the Disaster Mitigation Research Center at NIED prior to joining AIST. His current research interests include earthquake engineering, geomorphology, GIS, and application of remote sensing technology to disaster management.

Fumio Yamazaki is a Professor of urban environment systems at Chiba University, Chiba, Japan. He received his M.S. degree in civil engineering from the University of Tokyo in 1978. After working for Shimizu Corporation, Japan, and serving as a visiting scholar at Columbia University, he earned his Ph.D. degree in civil engineering from the University of Tokyo. Before joining Chiba University, Dr. Yamazaki was an Associate Professor at the University of Tokyo and a Professor at the Asian Institute of Technology, Bangkok, Thailand. His research interests include stochastic engineering mechanics, earthquake engineering, and more recently, application of GIS and remote sensing technologies to disaster management.